Absolute Intensities of the Vacuum Ultraviolet Spectra in Oxide Etch Plasma Processing Discharges

J. R. Woodworth, M. E. Riley, V. A. Amatucci, T. W. Hamilton, B. P. Aragon, Sandia National Laboratories, Albuquerque, New Mexico 87185-1423

Abstract

In this paper, we report the absolute intensities of ultraviolet light between 4.9 eV and 24 eV (250 nm to 50 nm) striking a silicon wafer in a number of oxide-etch processing discharges. Our emphasis is on photons with energies greater than 8.8 eV, which have enough energy to damage SiO_2. These discharges were in an inductively-driven Gaseous Electronics Conference reference cell which had been modified to more closely resemble commercial etching tools. Comparisons of measurements made through a side port in the cell and through a hole in the wafer indicate that the VUV light in these discharges is strongly trapped. For the pure halocarbon gases examined in these experiments (C_2F_6, CHF_3, C_4F_8), the fluxes of VUV photons to the wafer varied from 1 x 10^{15} to 3 x 10^{15} photons/cm^{2}sec or equivalently from 1.5 to 5 mW/cm^2. These measurements imply that 0.1% to 0.3% of the rf source power to these discharges ends up hitting the wafer as VUV photons for our typical 20 mT, 200 W rf discharges. For typical "ashing" discharges containing pure oxygen, the VUV intensities are slightly higher – about 8 mW/cm^2 . As argon or hydrogen diluents are added to the fluorocarbon gases, the VUV intensities increase dramatically, with a 10/10/10 mixture of Ar/ C_2F_6/ H_2 yielding VUV fluxes on the wafer 26 mW/cm^2 and pure argon discharges yielding 52 mW/cm^2 . Adding an rf bias to the wafer had only a small effect on the VUV observed through a side-port of the GEC cell.

DISCLAIMER

Introduction

For many years, there has been concern that plasma etching processes used to manufacture microelectronic circuits may also cause damage to the thin SiO_2 insulating layers in the circuits being fabricated.[1,2,3,4,5] This concern has become more acute as the feature sizes and insulator thickness in microelectronic circuits continue to shrink. Microcircuits can be damaged by energetic ions,[6,7,8] by electrons,[9] by metastable atoms[10], or by energetic photons from the vacuum ultraviolet[5,11,12,13,14,15,16] to the gamma ray[17,18] range. In addition, plasma nonuniformities can be a source of charging damage to microelectronic circuits[19,20,21]. This fact, in addition to the desire for process uniformity, has led plasma etching tool manufacturers to design inductively-coupled reactors, in which the ion energies and fluxes can be varied independently and in which the plasma is very uniform across the wafer surface[22]. All of the work described in this paper is in an inductively – coupled reactor.

Vacuum ultraviolet photons with energies greater than the 8.8-eV band gap energy in SiO_2 will be absorbed in the SiO_2 producing electron-hole pairs and E′ defect centers. An E′ center is formed by a silicon atom which is bonded only to three oxygen atoms and hence, has one dangling bond.[23] The holes may become trapped near Si/SiO_2 interfaces causing degradation in device characteristics such as dielectric breakdown[20], declines in the lifetime for minority carriers, and a flatband voltage shift in transistors.[15, 17] Joshi et. al have measured the surface and bulk conductivity resulting from absorption of these VUV photons.[24] [25] E′ centers in SiO_2 can absorb light at energies as low as 5.8 eV, making the device much more susceptible to damage[26]. Several authors have

reported vacuum ultraviolet spectra of plasma sources related to microelectronic processing.[15,27,28] We have previously reported absolute intensities of the vacuum ultraviolet spectra in high-density, inductively-coupled, aluminum etch microelectronic processing discharges[29] and have discussed possible damage mechanisms.

In all of the experiments that we are aware of, VUV fluxes to the wafer in plasma processing reactors have been estimated by looking through a port in the reactor sidewall. While looking though a port in the sidewall is experimentally convenient, it may not give accurate estimates of the VUV flux to the wafer due to non-uniformities in the discharge and radiation trapping of the VUV light inside the discharge. For this reason, we directly compare VUV fluxes measured through a hole in the wafer being etched with estimates made from measurements looking through a hole in the reactor sidewall. In this article, we report absolute intensities of VUV and near ultraviolet emission lines (4.9 – 24 eV) for oxide etching discharges in an inductively driven Gaseous Electronic Conference Reference Cell (GEC cell) [30 31]. In this GEC cell, we report VUV fluxes to the wafer as a function of pressure, gas mixture, and rf excitation level. For the measurements made through a port in the sidewall, we also report the effect of an rf bias on the wafer.

II. Apparatus

A. GEC Cell

Our Experiments were carried out in a GEC cell modified to produce inductively coupled discharges.[27 28] The GEC reference cell was designed as a standard research reactor

which would closely resemble commercial etching reactors but allow good access for a variety of diagnostics. The use of this reactor allows researchers at many different laboratories to directly compare their results. In addition to the large number of diagnostic ports, the GEC reference cell differs from many commercial plasma etching reactors in that it has a large "dead area" inside the vacuum that is not directly excited by the rf source and that it has grounded stainless steel walls. Figure 1 shows a detail of the rf excitation region of our GEC cell as modified for these experiments. Radio-frequency energy at 13.56 MHz was coupled from a 5 turn spiral coil through a quartz window to the discharge region. A 15.25-cm diameter silicon wafer rested on the lower electrode although only the central ~11 cm of the wafer was exposed to the main etching discharge. The distance from the wafer to the quartz window (Z in Fig. 1) was 3.9 cm for the measurements with the spectrometer located at a side-port of the cell and 4.5-cm when the spectrometer looked through a hole in the wafer. Thus, we might expect the discharge to be slightly "hotter" for the side-view measurements since the same amount of rf energy was being deposited in a slightly smaller volume. For some of the measurements, 13.56 MHz energy was also used to provide both rf and DC biasing of the wafer. The peak-to-peak voltage rf bias voltage on the wafer was measured with a capacitive voltage monitor that was fabricated at Sandia Labs and affixed to the back of the exposed edge of the wafer chuck. DC bias voltages were measured with a resistive divider and a DC voltmeter.

Most commercial oxide etching tools have insulating surfaces exposed to the plasma. We therefore surrounded as much of our discharge as possible with insulators by using an

anodized aluminum ring to hold the window in place and by suspending a 19 mm thick quartz ring from the window holder. A 9.6-mm-tall, 15.8-mm-wide notch was cut in one area of the quartz ring to give the VUV spectrometer an unimpeded line of sight to the discharge when the spectrometer was looking at the discharge from the side (Fig. 2) .

When the spectrometer viewed the discharge from below, a silicon wafer with a 6.3-mm diameter central hole was placed on the lower electrode to expose the spectrometer entrance slit, which was built into the surface of a special lower electrode. This lower electrode functioned as the entrance arm of the spectrometer when the discharge was viewed from below (Fig. 3). We had no ability to apply an rf or DC bias to this special lower electrode and hence, all VUV fluxes measured looking through a hole in the wafer are with a grounded lower electrode.

B. Spectrometer

The spectrometer used in these experiments was a 0.5-meter focal-length spectrometer of the Seya-Namioka (SEYA) design[32 33] Schematics of this spectrometer attached to the GEC cell are shown in Figs. 2 and 3. The SEYA had a single curved diffraction grating as its sole optical element. This grating, which was gold coated and had 1200 lines/mm, both diffracted the light and focused it to the exit slit. No window materials exist that will pass light at energies above 11 eV. We therefore coupled the spectrometer directly to the GEC cell through a two-stage differential pumping system as shown in Figs. 2 and 3. The SEYA viewed a relatively narrow cone of light with an F number of 20. In the side view, this 11-cm-long cone was centered 1.9 cm above the wafer surface and passed

above the center of the lower electrode. The through-the-wafer measurements viewed a 4.5-cm-long, F/20 cone of light located in the center of the discharge, between the lower electrode and the quartz rf coupling window. It is important to note that the side-view and through-the-wafer view measurements were not looking at identical parts of the discharge. Thus, discharge non-uniformities may cause us to predict different VUV fluxes at the wafer based on the two different measurements.

The entrance slits used in these experiments were 25-micron wide, 3-mm tall slits laser drilled into stainless steel foils. Due to the complex imaging properties of the Seya[29] we made no attempt to maximize resolution, but used exit slits 1-cm tall and 250 microns wide. These entrance and exit slit settings produced "flat topped" spectral lines, considerably simplifying the determination of absolute VUV fluxes.

Previous experience had taught us that small amounts of process gases can significantly damage the diffraction grating in the SEYA. We therefore took two additional precautions to keep reactive gases out of the spectrometer. In the "side-view" setup, a small, sonic, neon flow jet[34 35]was located directly behind the spectrometer entrance slit. This jet was driven by a room-temperature neon reservoir held at 0.3 Torr, which passed ~17 sccm of neon through a 1-mm by 10-mm "converging nozzle" aerodynamic slit. The system was designed so that each process gas molecule passing through the spectrometer entrance slit would suffer several collisions with neon atoms while passing through the neon jet, becoming entrained in the neon flow and exhausted out the pumps rather than entering the spectrometer. The stages of differential pumping between the

neon jet and the spectrometer allowed us to keep the spectrometer, which was exhausted by a 170 liter/sec turbomolecular pump, at ~1 x 10^{-5} Torr while the neon was flowing. At most wavelengths, the sensitivity of the SEYA spectrometer plus detectors changed by less than 10% during the course of the side-view experiments, indicating that the neon jet was successful in protecting the system from degradation.

We were not able to incorporate the neon flow jet into the system that viewed the discharge through the hole in the wafer. The plasma sheath above the wafer typically generates well-collimated beams of ions with 15 – 40 eV of energy which strike the wafer surface. To keep this beam from passing through the spectrometer entrance slit and then damaging the grating by ion-beam milling, we biased an intermediate slit in the differential pumping system at + 40 V DC to repel the ions. A 92% open, 1.9 line per mm screen was welded across the intermediate slit to assure that the voltage on this slit would not simply lens the ions through the slit. The sensitivity of the SEYA plus detectors degraded by about a factor of three during the through-the-wafer experiments, indicating that the biased electrode and differential pumping system were not successful in protecting the spectrometer optics. This degradation caused the major uncertainty in the VUV fluxes given in this paper.

C. Spectrometer Calibration

Two photon detectors were used in these experiments. A "Channeltron^{TM}" channel electron multiplier[36] was placed behind the exit slit to measure photons with energies

from 8 eV to 24 eV. A photomultiplier tube with a magnesium fluoride window and a cesium telluride photocathode was used to detect photons having energies from 4 eV to 11 eV.

To calibrate the sensitivity of the SEYA plus detectors, we coupled the entrance slit of the SEYA to the exit slit of a 1-meter focal length spectrometer as shown in Fig. 4. This 1-meter spectrometer, with various light sources, was used to provide a monochromatic input beam to the SEYA. An aperture plate placed over the grating in the 1-meter spectrometer assured that all of the light passing into the SEYA actually struck the Seya's diffraction grating. At each calibration wavelength, the intensity of the light entering the SEYA was measured with a photodiode calibrated by the National Institute of Standards & Technology (NIST).[37] The NIST photodiode was mounted so that it could be moved into or out of the beam at a location between the SEYA's entrance slit and grating. Comparing the intensity measured with the NIST photodiode to the signal produced by the channeltron or photomultiplier at the SEYA exit slit allowed us to determine the sensitivity of the SEYA + detector system. These calibrations were performed before and after each set of VUV flux measurements and the before and after measurements were averaged to provide a mean sensitivity for each run.

Two light sources were used to provide UV light for the calibrations. A windowless, rf-excited discharge lamp built at Sandia (shown in Fig. 4) was used to provide eight intense resonance lines of the noble gases, from helium at 58.4 nm to Xe at 147 nm as well as hydrogen lines at 121.6 nm and 160.8 nm. There was one stage of differential

pumping between this lamp, which was typically operated at 80 mTorr and the 1-meter spectrometer which operated at ~ 10^{-5} Torr. A microwave-excited mercury lamp[38] was used to provide spectra at 184.9 nm and 254 nm. Over the wavelength range of interest, the sensitivity of the SEYA plus channeltron varied by a factor of 35 and the sensitivity of the SEYA plus photomultiplier tube varied by a factor of two. These strong variations in sensitivity with wavelength show the importance of calibrating the system.

D. Calculation of VUV Fluxes:

Using the signals from the detectors and the known sensitivity of the SEYA + detector combination, we derived the wavelength-dependent flux of photons in the cone of light passing through the SEYA's entrance slit and striking the grating. For our ~f/20 spectrometer, this cone of light subtended a solid angle of 2.6 x 10^{-3} steradians. We then calculated the number of photons an elemental area of the discharge radiated into 4π steradians. The number of photons from a particular species radiated per steradian by an elemental volume da x dl (see Fig 5) is given by

$$I = N(A_{12} /4\ \pi)\ da\ dL \qquad 1$$

Where N = number of excited states/cm^3 and A_{12} = transition rate for the excited state to ground state transition. The number of photons per second passing through the spectrometer entrance slit (I') is then given by the brightness of the elemental area multiplied by the solid angle subtended by the slit:

$$I' = (NA_{12} /4\ \pi)\ da\ dL\ (A_s/L^2) = (NA_{12}/4\ \pi)\ (da/L^2)\ A_s\ dl \qquad 2$$

Where A_s = Area of slit and L = distance from the elemental area to the slit. Note that da/L^2 is the solid angle ($d\omega$) subtended by the elemental area dadL from the position of the slit. Hence:

$$I' = (NA_{12}/4\pi)A_s d\omega dL \qquad 3$$

To obtain the total number of photons passing through the slit and striking the grating (I_g) in terms of elemental source brightness, we must integrate over solid angle and over the length of the discharge column.

$$I_g = \int dL \int d\omega\, (NA_{12}/4\pi)A_s \qquad 4$$

The limit on the solid angle is set by the solid angle subtended by the diffraction grating as seen by the slit:

$$\Omega = A_g / F^2 \qquad 5$$

Where A_g = area of grating and F = distance from slit to grating. The limit on the L integral is set by the length of the discharge column as viewed by the spectrometer. Note that L will hence be different for the side-view and the through-the-wafer-view calculations. Thus, the total number of photons from a particular transition in the discharge passing through the slit and striking the grating is:

$$I_g = (NA_{12}/4\pi)^*(A_s A_g/F^2) \qquad 6$$

In order to calculate the VUV flux at the wafer, we approximated the discharge as a uniformly emitting cylinder 5.7 cm in radius (R_o) and 4.5 cm tall (Z_o). The intensity at the wafer (I_w) , is given by the following integral in cylindrical coordinates:

$$I_w = (NA_{12}/4\pi) \int r dr \int d\Phi \int dz\, [\, z /(z^2 + r^2)^{3/2}] \qquad 7$$

Where the limits of integration are 0 and R_o= 5.7 cm for r; 0 and 2 π for Φ; and 0 and Z_o = 4.5 cm for z. Solving the integral we obtain:

$$I_w = (NA_{12}/2)\,[R_o + Z_o - (R_o^2 + Z_0^2)^{1/2}] \qquad 8$$

Solving equation (6) for NA_{12} and substituting the resulting expression for NA_{12} into equation (8) allows us to derive expressions for the intensity at the wafer in terms of the number of photons striking the grating:

$$I_w = [(2\,\pi\, I_g F^2)/(LA_sA_gT_s)]*[R_o+Z_o - (R_o^2+Z_o^2)^{1/2}] \qquad 9$$

Where T_s is the transmission of the 92% open screen used when the spectrometer was looking through a hole in the wafer. Our calibrations of the spectrometer plus detectors allowed us to determine I_g for each spectral line and hence allowed us to determine the intensity at the wafer (I_w). For the side view measurements, when we were looking through a 11-cm length of discharge we set L = 11 cm. For the through-the-wafer measurements, when we were looking up through a 4.5-cm thickness in the center of the discharge, we set L = 4.5 cm.

III. Results

In this section we present VUV spectra and intensities for discharges in the GEC cell for pure C_2F_6 (Hexafluoroethane), CHF_3 (Trifluoromethane), C_4F_8 (Octofluorocyclobutane) , oxygen, argon, and mixtures of C_2F_6 with argon and hydrogen. Our normal operating conditions were 20 mTorr total pressure, 10 sccm of gas flow for each gas species and 200 Watts of rf induction power. Hebner and Miller[39]

have previously reported electron densities and temperatures of $n_e = 3 \times 10^{11}/cm^3$ and $T_e = 4$ eV for nominally identical discharges in C_2F_6, CHF_3, and C_4F_8.

Figure 6 shows the spectrum of a 50/50 argon / C_2F_6 discharge mixture from 70 nm (17.6 eV) to 250 nm (4.9 eV) as viewed through a hole in the silicon wafer. Figure 6 shows the intensity of spectral lines striking the wafer in units of 10^{14} photons/cm^2sec. The spectrum is dominated by strong neutral argon lines at 104.8 and 106.6 nm. In addition to these lines, a number of lines of fluorine appear between 79 and 98 nm, carbon lines are scattered throughout the spectrum[40] and molecular CF bands appear at longer wavelengths[41]. Weak emission features between 130 and 190 nm are probably due to the fourth positive band system[35] of the CO molecule. The most likely source of oxygen in the discharge is etching of the quartz window and ring. All of the emission features seen in these experiments are of neutral atoms or molecules. No lines of ionic species were identified. Table I summarizes the locations of the brighter lines seen in this spectrum. Lines with an energy greater than 8.8 eV (shorter than 140 nm) have enough energy to damage silicon dioxide.

Figure 7 shows a spectrum of 20 milliTorr discharge in pure CHF_3 discharges. This figure compares intensities at the center of the wafer as calculated from data looking from the side of the discharge versus looking through a hole in the wafer. In addition to the lines seen in Fig. 6, this spectrum shows the Lyman series alpha and beta lines of neutral hydrogen at 121.6 and 102.6 nm. It is readily apparent that the measurements made

through a hole in the wafer predict much higher VUV fluxes striking the wafer than measurements made from the side of the discharge do.

Figure 8 shows a spectrum looking though the wafer at a pure C_4F_8 discharge. This discharge is at relatively low pressure (10 milliTorr) and high rf inductive power (300 W) and shows the triplet of fluorine lines near 80 nm and the overlapping fluorine lines between 95 and 97 nm clearly. In addition to the carbon and probably CO lines, a weak oxygen line is visible at 130.4 nm. Under circumstances discussed later, this oxygen line can dominate the entire spectrum.

In this section we present tables giving the VUV fluxes to the wafer for a number of different conditions. Figure 9 shows a plot of absorption coefficient and 1/e photon penetration depth of VUV light in amorphous SiO_2 calculated from work by Philip.[42] In the analysis in this paper we divide this absorption spectrum into two regions of interest. At wavelengths shorter than ~130 nm, absorption coefficients are large and penetration distances are small – 10 to 100 nm. Between 130 and 140 nm penetration distances are much larger – 100 to 1000 nm. Above 140 nm, photons are not likely to damage SiO_2. Damage mechanisms can be quite different depending on whether the VUV energy is deposited near the surface of the SiO_2 or in depth[26]. In the tables that follow therefore, we have divided VUV fluxes to the wafer into two regions, wavelengths shorter than 130 nm and wavelengths between 130 and 140 nm.

Table II shows VUV fluxes to the wafer in pure C_4F_8 discharges as calculated from measurements through a hole in the wafer for a flow rate of 10 sccm. The wafer was

grounded for these measurements. This table shows that VUV fluxes decrease as the pressure increases and increase with increasing rf power. There is one anomalous point in the 20 mTorr, 200 Watt data between 130 and 140 nm. This flux was high because of a bright oxygen line at 130.4 nm. Although no oxygen was supplied to the chamber while this spectrum was being recorded, we had cleaned the cell with an oxygen discharge immediately before this spectrum was taken. Oxygen diffusing out of coatings on the stainless steel walls was enough to completely dominate the emission spectrum in the VUV.

Table III shows VUV fluxes at the wafer based on measurements through the hole in the wafer for pure C_2F_6 discharges as a function of pressure at 200 Watts rf source power and a flow rate of 10 sccm. Again, the fluxes decrease as pressure increases. Increases in collisions, which can quench the high lying states leading to VUV emissions probably explain the decrease in VUV fluxes at high pressure.

Table IV shows the effect of adding argon and hydrogen diluent gases to C_2F_6. In Table IV the wafer was grounded, the total pressure was 20 mTorr and the rf power was 200 Watts. Table IV lists results for a pure C_2F_6 discharge with a 10 sccm flow, a discharge mixture with 10 sccm of Ar and 10 sccm of C_2F_6, and a discharge having a 10 sccm flow of each of Ar, H_2, and C_2F_6 Adding diluents increases VUV fluxes to the wafer by more than an order of magnitude. For argon, the increase is entirely due to the two argon resonance lines at 104.8 and 106.6 nm. For hydrogen, the increase is partly due to the strong atomic hydrogen line at 121.6 nm but is mainly due to the thousands of molecular

hydrogen lines that occur between 80 and 165 nm[43 44]. These lines merged into a ragged "background level" in our spectra and we simply averaged that background level to determine the VUV flux from the H_2 emissions.

Table V compares intensities at the wafer as calculated from side-view and through-the-wafer view measurements using equation 9. For all of these discharges, the total pressure was 20 mTorr, the flow rate of each gas species was 10 sccm and the rf inductive power was 200 W. For oxygen and the oxide etch discharge mixtures, the intensities calculated at the wafer from the through-the-wafer measurements are at least a factor of three higher than the intensities calculated from the side-view measurements. For the argon discharges, the intensity calculated at the wafer is a factor of 15 higher using the through-the-wafer measurements than using the side-view measurements. Further, ratios of individual lines are even more different in the side- and through-the-wafer views. The calculated argon 104.8-nm line intensity on the wafer increases by a factor of 100 when we switch from the side-view to the through-the-wafer data. While some part of these discrepancies may be due to the fact that the side-view and through-the-wafer-view did not observe identical parts of the discharge, it is likely that most of the discrepancies are due to optical trapping. For many of the spectral lines, the VUV photons are being emitted and reabsorbed many times before they eventually escape from the discharge. This radiation trapping [45,46, 47, 48] can lengthen the effective radiative lifetime of the excited state that produces the photon dramatically. This, in turn, gives non-radiative quenching processes much more time to quench the excited state before it emit a VUV photon. As a result, the VUV photon flux is not at all uniform across the discharge and

varies in a detailed way on the local number densities and temperatures of the various excited states and quenching species. These considerations make it very difficult to accurately predict the VUV flux striking the wafer unless the VUV flux measurements are actually made through a hole in the wafer as they were in these experiments.

Table VI compares calculated intensities at the wafer using "side-view" data with and without an rf bias on the wafer. This data shows that the rf bias has surprisingly little effect on the VUV flux levels. For both gas mixtures (CHF_3 and an Ar/ C_2F_6/ H_2 mixture) 100 Watts of net rf bias power was applied to the wafer, raising the total power supplied to the GEC cell by 50%. The several-hundred-Volt rf peak-to-peak bias measured on the wafer gives evidence that much of this rf bias power did reach the wafer. The VUV intensity calculated at the wafer, however, increased by only ~13% for the CHF_3 discharge and not at all for the Ar/ C_2F_6/ H_2 mixture. Since our "side-view " measurements are known to be affected by radiation trapping, it is not clear from this data whether the VUV intensity at the wafer is really unaffected by rf-biases on the wafer, or whether the measurements were simply compromised by radiation trapping. The ideal measurements would have looked at the effect of rf-biases using through-the-wafer data, but our apparatus used for the through-the-wafer view was not compatible with rf biasing.

IV. Summary:

We have examined the fluxes of UV radiation to the silicon wafer in an inductively driven GEC reference cell from 4.9 ev to 24 eV (250 nm to 50 nm) with particular emphasis on the energy range above 8.8 eV. At energies above 8.8 eV, VUV photons

can damage SiO_2. All the emission spectra observed in these experiments were from neutral atoms or molecules – no ion lines were observed. Also, no lines were observed at energies above 17 eV (73 nm). Because the absorption coefficient of SiO_2 varies strongly in this spectral region, some of the VUV photons with energies above 8.8 eV will be absorbed quickly – within 10 nm of the SiO_2 surface, while others may penetrate as much as a micron into the SiO_2 before being absorbed. The amount of VUV produced and its average absorption depth in SiO_2 depends in detail on the power, pressure and gas mixture of the discharge.

In these experiments, VUV fluxes were measured directly through a hole in the silicon wafer to minimize the effects of radiation trapping on the measurements. Process gases entering the spectrometer during the "through-the-wafer" experiments degraded the spectrometer's grating and detectors during the experiments. As a result of this degradation, the "centerpoint values" listed above can be multiplied or divided by a factor of 1.7 before reaching the limits of our uncertainties.

These experiments demonstrated that two stages of differential pumping and a biased electrode placed between the GEC discharge and the spectrometer were not adequate to protect the spectrometer from the reactive process gases. Adding a flowing neon jet in the middle of the differential pumping stages did prevent the process gases from degrading the spectrometer.

For the pure halocarbon gases examined in these experiments (C_2F_6, CHF_3, C_4F_8), measurements taken through a hole in the wafer indicated that the fluxes of VUV photons to the wafer varied from 1 x 10^{15} to 3 x 10^{15} photons/cm^{2}sec or equivalently from 1.5 to 5 mW/cm^2. These measurements imply that 0.1% to 0.3% of the rf source power to these discharges ends up hitting the wafer as VUV photons for our typical 20 mT, 200 W rf discharges. For typical "ashing" discharges containing pure oxygen, the VUV intensities are slightly higher – about 8 mW/cm^2 or ~0.5% of the rf source power. As argon or hydrogen diluents are added to the fluorocarbon gases, the VUV intensities increase dramatically, with a 10/10/10 mixture of Ar/ C_2F_6/ H_2 yielding VUV fluxes on the wafer 26 mW/cm^2 and pure argon discharges yielding 52 mW/cm^2 . These correspond to 1.6% and 4% of the rf source power striking the wafer for the Ar/ C_2F_6/ H_2 mixture and pure Ar respectively. These VUV fluxes to the wafer increased roughly linearly with increases in rf source power and decreased as pressure was increased.

In addition to measurements taken looking through a hole in the wafer, we measured VUV fluxes through a side-port of our GEC cell. These "side-view" measurements typically suggested VUV intensities at the wafer a factor of three lower than the "through-the wafer view" although some lines were as much as a factor of 100 dimmer when looking from the side. This discrepancy between side-view and through-the-wafer-view measurements suggest that the VUV light in these discharges is undergoing strong radiation trapping. RF-biasing the wafer had only a weak effect or no effect on the VUV emerging from the side of the discharge, but due to the radiation trapping, we can not be sure that the rf bias did not affect the VUV fluxes at the wafer.

V. Acknowledgments

The authors would like to acknowledge many helpful discussions on plasma physics of the discharge mixtures with Drs. G. A. Hebner and P. A. Miller at Sandia. We also wish to thank Mr. W. Tatum of Southwest Machining for his help in fabricating a number of unusual vacuum components used in these experiments. Sandia is a multiprogram laboratory operated by Sandia Corporation, a Lockheed-Martin Company, for the United States Department of Energy under Contract DE-AC04-94AL85000.

Table I: Emission lines identified in spectrum of Ar/C_2F_6 mixture

Wavelength (nm)	Element/Molecule
79.2	F
80.8	F
80.6 – 89.2	Ar
104.8	Ar
106.6	Ar
126.1	C
127.9	C
132.9	C
156.1	C
165.7	C
193.0	C
198.1	CF
202.6	CF
208.0	CF
213.6	CF

Table II: VUV fluxes to the wafer in pure C_4F_8 discharges with 10 sccm flow rate, based on measurements made through hole in wafer. Fluxes are in units of 10^{14} photons/cm^2sec at wafer surface and are summed over the wavelength intervals listed.

Pressure (mTorr)	Rf source power (Watts)	VUV Fluxes below 130 nm	VUV fluxes 130 – 140 nm	Total Flux 70 – 140 nm
10	160	2.0	0.9	2.9
10	200	5.0	3.6	8.6
10	300	18	6.5	24.5
20	160	1.2	0.3	1.5
20	200	5.5	25	30.5
20	300	7.7	2.8	10.5

Table III: VUV fluxes at wafer as calculated from view through hole in wafer; pure C_2F_6 discharges, 10 sccm flow rate, 200 W rf source power, grounded wafer. Fluxes are in units of 10^{14} photons /cm^2 sec striking the wafer and are summed over the wavelength intervals listed.

Pressure (milliTorr)	VUV Fluxes below 130 nm	VUV fluxes 130 – 140 nm	Total Flux 70 – 140 nm
10	13.8	7.0	20.8
20	8.3	2.8	11.1
50	5.1	4.5	9.6

Table IV: VUV fluxes to wafer in C_2F_6 discharges with diluent gases as calculated from view through hole in wafer. Fluxes are in units of 10^{14} photons /cm^2sec striking the center of the wafer and are summed over the wavelength intervals listed. Total pressure and rf power are 20 mT and 200 Watts respectively.

Gas	Flow Rate (sccm)	VUV Fluxes below 130 nm	VUV fluxes 130 – 140 nm	Total Flux 70 – 140 nm
C_2F_6	10	8.3	2.8	11.1
Ar/ C_2F_6	10/10	113	2.5	115.5
Ar/ C_2F_6/ H_2	10/10/10	166	10	176

Table V: Comparison of side-view and through-the-wafer view VUV intensities at the wafer. VUV fluxes are summed over the wavelength intervals listed.

gas	Flow rate (sccm)	view	VUV Fluxes below 130 nm	VUV fluxes 130 – 140 nm	Total Flux 70 – 140 nm
C_2F_6	10	Through wafer	8.3	2.8	11.1
C_2F_6	10	Side view	2.5	1.1	3.6
CHF_3	10	Through wafer	27	3.3	30.3
CHF_3	10	Side view	6.8	3	9.8
Ar/ C_2F_6/H_2	10/10/10	Through wafer	166	10	176
Ar/ C_2F_6/H_2	10/10/10	Side view	44	6.3	50.3
Ar	10	Through wafer	350	0.0	350
Ar	10	Side view	22	0.0	22
O_2	10	Through wafer	13.2	43	56.2
O_2	10	Side view	4.7	8	12.7

Table VI: Comparison of side-view VUV intensities with and without rf bias on wafer. Total pressure was 20 mTorr and rf inductive power was 200 Watts for this data. VUV fluxes are summed over the wavelength intervals listed. CHF_3 flow rates are 10 sccm. Flow rates for the $Ar/C_2F_6/H_2$ mixtures are 10/10/10 sccm.

gas	Rf bias power Watts	Rf bias peak to-peak Volts	DC bias Volts	VUV fluxes below 130 nm	VUV fluxes 130-140 nm	Total flux 70 – 140 nm
CHF_3	0.0	0.0	0.0	6	2.6	8.6
CHF_3	100 W	241 V	-23V	6.8	3	9.8
Ar/ C_2F_6/H_2	0.0	0.0	0.0	44	6.3	50.3
Ar/ C_2F_6/H_2	100 W	360 V	-23 V	44	6.3	50.3

Figure Captions:

Figure 1: Schematic of the discharge region in our inductively-driven GEC cell. RF inductive power is coupled from the spiral coil through the SiO_2 window to the discharge. The SiO_2 window, the anodized aluminum window holder, the SiO_2 ring and the Si wafer surround the plasma with insulating or semiconducting surfaces. For the side-view measurements, the spectrometer looked through the notch in the SiO_2 ring. For the through-the-wafer measurements, the lower electrode shown was replaced with a grounded lower electrode that contained the spectrometer entrance slit. All dimensions in the figure are in mm. The distance 'Z' between the wafer and the window was 39 mm for the side-view experiments and 45 mm for the through-the-wafer experiments.

Figure 2: Schematic of SEYA spectrometer attached to GEC cell for "side-view" measurements. Two stages of differential pumping and a neon flow jet prevented the reactive gases from the GEC cell from entering the spectrometer.

Figure 3: Schematic of SEYA spectrometer attached to GEC cell for "through-the-wafer" measurements. Two stages of differential pumping and a biased intermediate electrode were designed to prevent the reactive gases from the GEC cell from entering the spectrometer.

Figure 4: Schematic of apparatus used to absolutely calibrate the sensitivity of the SEYA spectrometer in the VUV. Light from the discharge was passed through the 1-meter spectrometer to provide a monochromatic input beam to the SEYA. The NIST diode measured the absolute flux of photons entering the SEYA.

Figure 5: Geometry for determining the number of photons radiated by an elemental volume dadL that pass through the solid angle subtended by the spectrometer entrance slit (A_s).

Figure 6: Spectrum of a 20 milliTorr, 200 Watt discharge in the GEC cell containing a 50/50 mixture of argon and C_2F_6. Intensities are given in terms of photons/ cm^2 sec striking the center of the wafer. The two strong Ar lines peak off scale at approximately 50 x 10^{14} photons/cm^2sec. A number of fluorine and carbon lines occur at energies above 8.8 eV, the energy threshold for damage in SiO_2. These measurements were taken through the hole in the wafer.

Figure 7: Spectra for pure CHF_3 discharges at 20 mTorr pressure and 200 W rf. This plot compares intensities at the wafer as calculated from "side-view" measurements (solid curve) and "through-the-wafer measurements" (dashed curve).

Figure 8: Spectrum of 10 mTorr, 300 Watt rf, pure C_4F_8 discharge viewed through a hole in the wafer. In this low pressure high-power discharge all of the fluorine lines between 75 and 98 nm are clearly visible. The weak oxygen impurity line at 130.4 nm can dominate the spectrum under some circumstances.

Figure 9: Plot of absorption coefficients and 1/e penetration depths for VUV photons in amorphous SiO_2. Photons with wavelengths shorter than ~140 nm can damage SiO_2. Below 130 nm, the 1/e penetration depths are relatively small – 10 to 100 nm. Between 130 and 140 nm, the penetration depths are larger 100 nm to 1 micron.

[1] G. S. Oehrlein, Materials Science and Engineering **B4**, 441, (1989)

[2] K. H. Ryden, H. Norstrom, C. Nender and S. Berg, J. Electrochem. Soc.: Solid State Science & Technology, **134**, 3113, (1987)

[3] A. W. Flounders, S. A. Bell, D. W. Hess, J. Electrochem. Soc, **140**, 1414, (1993)

[4] P. A. Miller, D. M. Fleetwood and W. K. Schubert, J. Appl. Phys, **69**, 488, (1991)

[5] T. Tatsumi, S. Fukuda, and S. Kadomura, Jpn. J. Appl. Phys, **32**, 6114, (1993)

[6] C. Cardinaud, G. Turban, B Grolleau, J. P. Grandchamp, C. Lejeune, P. Scheiblin, and E. Collard, Applied Surface Science, **36**, 332, (1989)

[7] S. Yokoyama, Z. J. Radzimski, K. Ishibashi, S. Miyazaki, M. Hirose, Jpn. J. Appl. Phys, **33,** Part 1, 2179, (1994)

[8] K. Yokogawa, Y. Yajima, T. Mizutani, Jpn. J. Appl. Phys, 30, 3199, (1991)

[9] T. Yunogami and T. Mizutani, J. Appl. Phys, **73**, 8184, (1993)

[10] T. Ono, N. Itabashi, I. Ochiai, S. Yamamoto, K. Mochiji, Jpn. J. Appl. Phys, 36, Part 1, 6718, (1997)

[11] T. Mizutani, S. Nishimatsu, T. Yunogami, Materials research Society Symposium Proceedings, **128**, 605, (1989)

[12] T. Kang, S. Ueng, B. Dai, L. Chen, H. Cheng, Jpn. J. Appl. Phys **34**, Part 1, 2272, (1995)

[13] T. Yunogami, T. Mizutani, K. Tsujimoto, and K. Suzuki, Jpn. J. Appl. Phys, 29, Part 1, 2269,(1990)

[14] K. Yokogawa, Y. Yajima, T. Mizutani, S. Nishimatsu, K. Suzuki, Jpn. J. Appl. Phys, 29, Part 1, 2265, (1990)

[15] T. Yunogami, T. Mizutani, K. Suzuki, and S. Nishimatsu, Jpn. J. Appl. Phys, **28**, 2172, (1989)

[16] T. Tatsumi, S. Fukuda, S. Kadomura, Jph. J. Appl. Phys, **33**, Part 1, 2175, (1994)

[17] C. M. Dozier, D. B. Brown, IEEE Trans on Nuclear Sci. **NS-28**, 4137, (1981)

[18] C. M. Dozier, D. B. Brown, R. K. Freitag, and J. L. Throckmorton, IEEE Trans on Nuclear Sci. **NS-33**, 1324, (1986)

[19] S. Fang and J.P. McVittie, J. Appl. Phys **72**(10), 4865, (1992)

[20] S. Fang and J. P. McVittie, Appl. Phys. Lett, **62**, 1507, (1993)

[21] S. Murakawa, J. P. McVittie, Jpn. J. Appl. Phys, **33**, Part 1, 2184, (1994)

[22] S. Ma, M. Jain, J. D. Chinn, J. Vac. Sci. Technol. A, **16**, 1440, (1998)

[23] T. P. Ma, P. V. Dressendorfer, Ionizing Radiation Effects in MOS Devices and Circuits, P. 57, Wiley, New York, 1989

[24] M. Joshi, J. P. McVittie, K. Saraswat " Direct Experimental Determination and Modeling of VUV Induced Bulk Conduction in Dielectrics during Plasma Processing" Proceedings of the Plasma Process induced Damage Conf. May , 2000, Santa Clara CA, available on line from www.chapters.vacuum.org//nccavs/order.html or from mcvittie@stanford.edu.

[25] M. Joshi, J. P. McVittie, K. Saraswat, "Measurement of VUV induced surface conduction in dielectrics using synchrotron radiation, IBID.

[26] D. L. Griscom and W. B. Fowler, Proceedings of the International Topical Conference on MOS Insulators, Raleigh, NC, (1980) p. 97, Pergamon Press, NY, NY. ISBN 0-08-025969-3

[27] A. C. Fozza, A. Kruse, A. Hollander, A. Ricard, M. R. Wertheimer, J. Vac. Sci. Technol. A, **16**, 72 (1998)

[28] S. Miyake, W. Chen, T. Ariyasu, Jpn, J. Appl. Phys, **29**, 2491, (1990).

[29] J. R. Woodworth, M. G. Blain, R. L. Jarecki, T. W. Hamilton, B. P. Aragon, J. Vac. Sci. Technol A **17(6)**, 3209, (1999)

[30] P. J.Hargis et. al. Rev. Sci Insstum. 65,140, (1994)

[31] P. A. Miller, G. A. Hebner, K. E. Greenberg, P. D. Pochan, and B. P. AragonJ. Res. Natl. Inst. Stand. Technol. 100, 140 (1994)

[32] Experimental Methods in the Physical Sciences, Vol 32: Vacuum ultraviolet Spectroscopy II, J. A. Samson and D. L. Ederer, Academic Press, New York, (1998)

[33] McPherson Instruments Corporation, Acton Massachusetts

[34] A. H. Shapiro, The Dynamics and Thermodynamics of Compressible Fluid Flow, Vol. I, Wiley, New York, 1953 P. 83.

[35] G. W. Van Wylen and R.. E. Sonntag, Fundamentals of Classical Thermodynamics, 3rd Edition, Wiley, New York, 1985, pp. 571, 650 and 712

[36] Galileo Electro-optics Corp. Sturbridge, Massachusetts

[37] R. E. Vest, National Institute of Standards and Technology, Gaithersburg, MD, rvest@nist.gov

[38] Opthos Instruments, Rockville, Maryland (301) 926-0589

[39] G. A. Hebner and P. A. Miller, Journal of Applied Physics, in Press, July 2000

[40] NIST Atomic Spectra Database, available on the internet at http://www.physics.nist.gov

[41] Spectroscopic Data, Vol 1, Heteronuclear Diatomic Molecules, S. N. Suchard, IFI/Plenum, New York, 1975

[42] H. R. Philip, Absorption coefficients of silicon dioxide, Handbook of Optical Constants of Solids, Ed. E. D. Palik, Academic Press, New York, 749 (1985)

[43] J. Junkes, E. W. Salpeter and G. Milazzo, Atomic Spectra in the Vacuum Ultraviolet from 2250 to 1100 Å, Pt. One, (Specola Vaticano, Citta del Vaticano), 1965

[44] J. A. R. Samson, Techniques of vacuum Ultraviolet Spectroscopy, p. 139, Wiley, New York, 1967

[45] T. Holstein, Phys. Rev. **72**, (12), 1212, (1947)

[46] J. Huennekens and T. Colbert, J. Quant. Spectros. Radiat. Transfer **41**, (6) 439, (1989)

[47] T. Holstein, Phys. Rev. **83** (6), 1159,(1951)

[48] M. E. Riley, W. J. Alford, Radiation Trapping in Plasmas, Sandia Report SAND95-1201. UC-401, June 1995

Figure 1, J. R. Woodworth, et. al. JVSTA

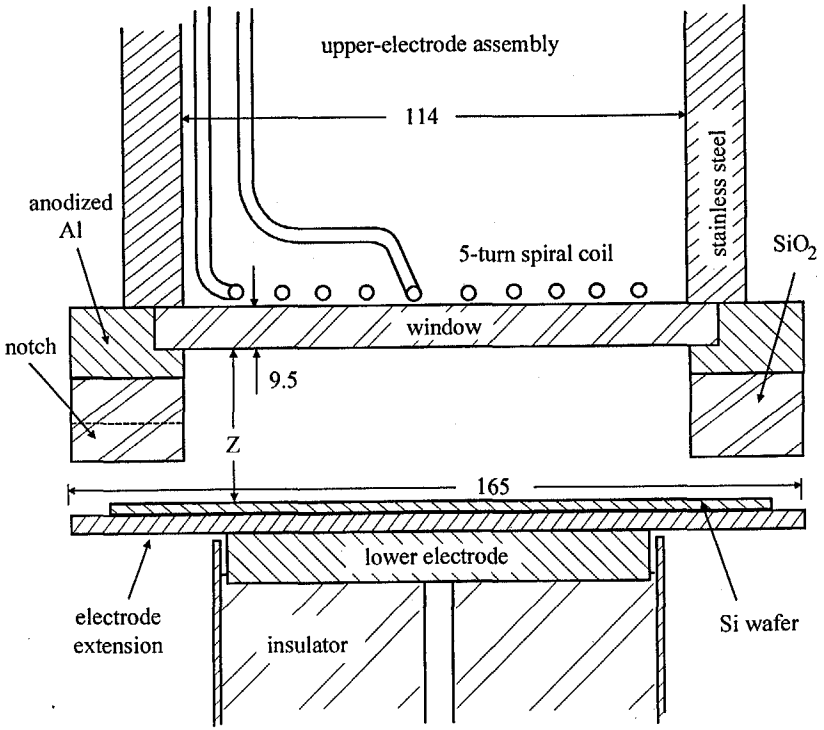

Figure 2

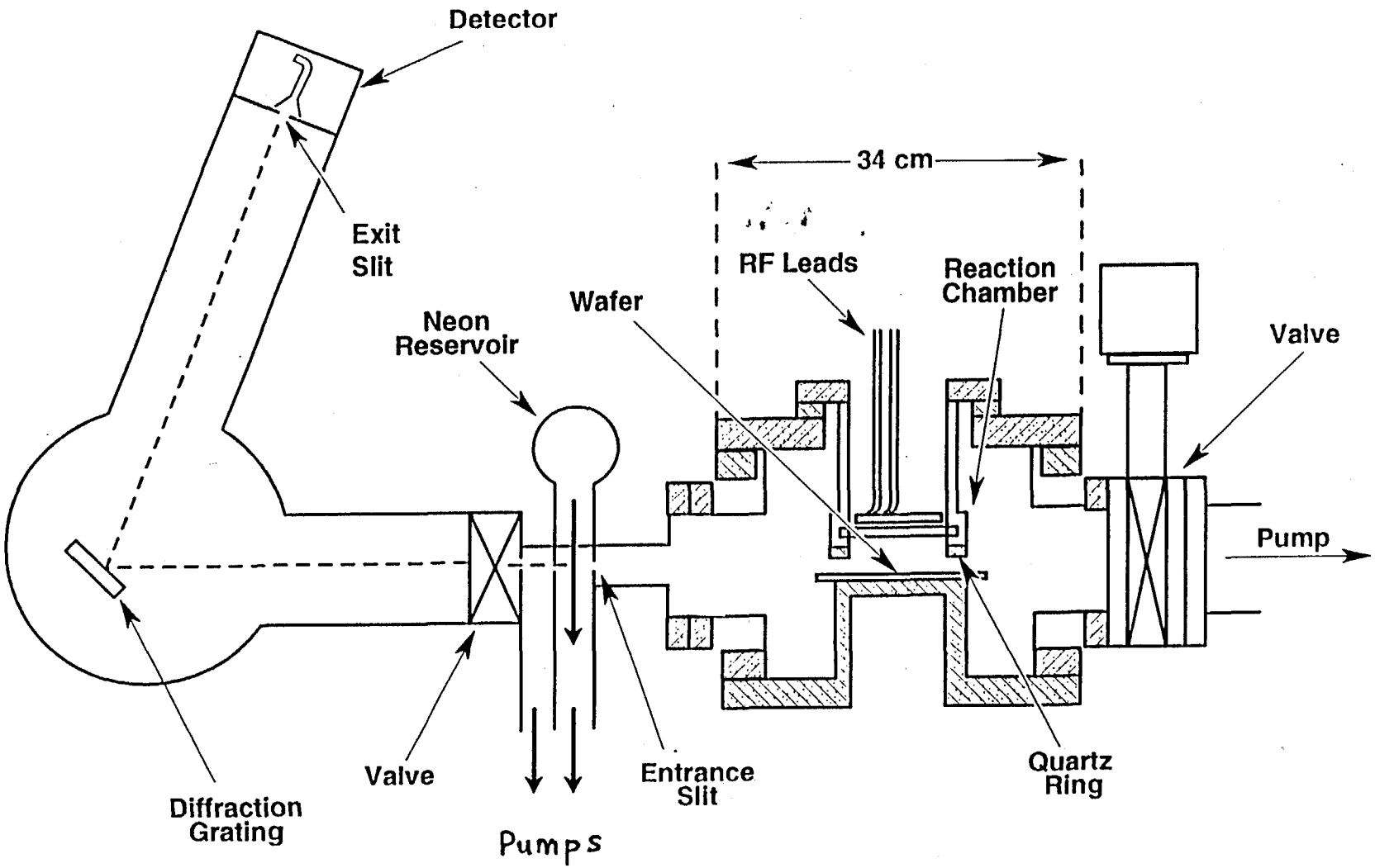
Detector
Exit
Slit
34 cm
RF Leads
Reaction
Chamber
Wafer
Neon
Reservoir
Valve
Pump
Diffraction
Grating
Valve
Entrance
Slit
Quartz
Ring
Pumps

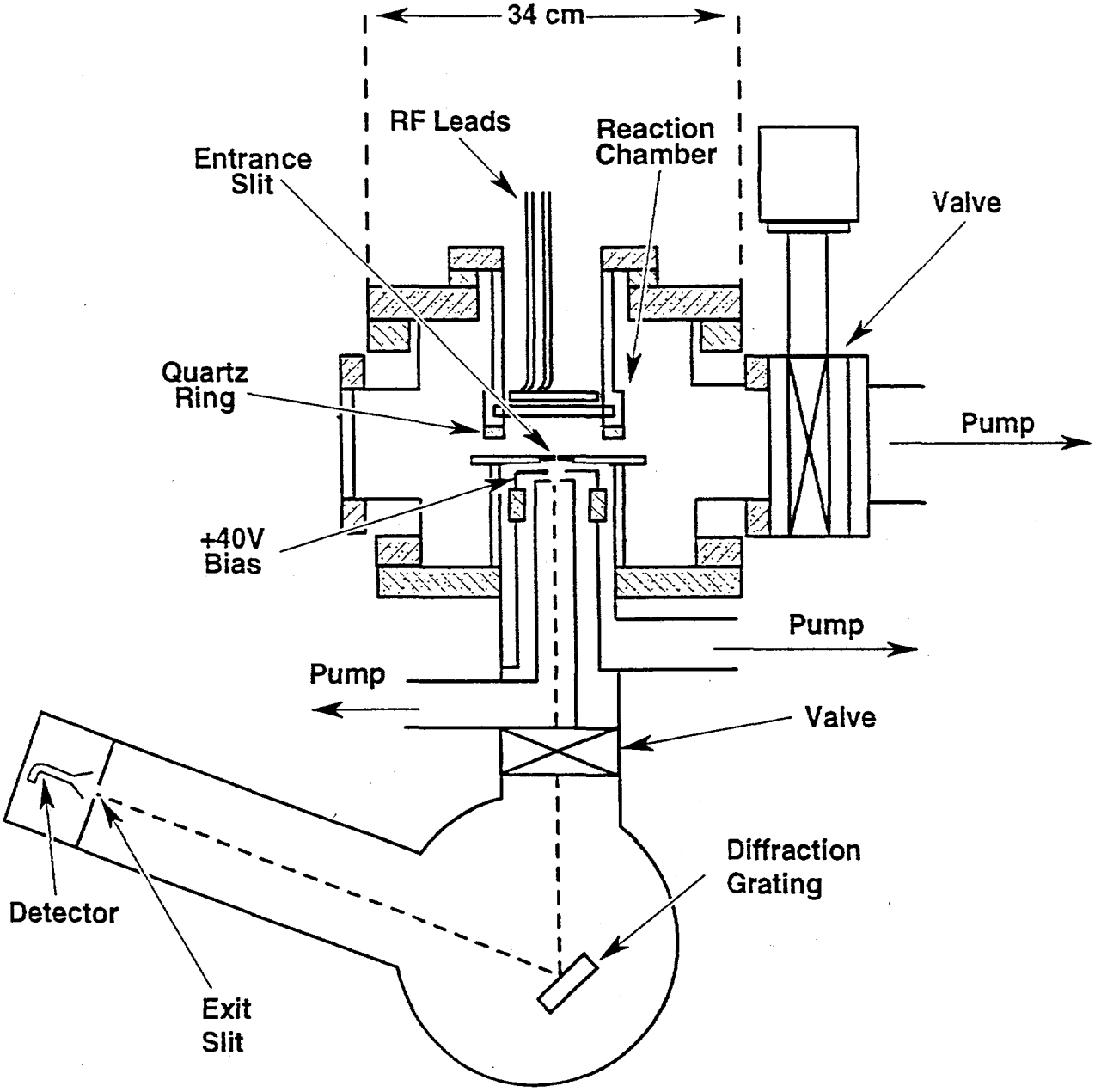
34 cm
RF Leads
Reaction Chamber
Entrance Slit
Valve
Quartz Ring
Pump
+40V Bias
Pump
Pump
Valve
Diffraction Grating
Detector
Exit Slit

Figure 4, J. R. Woodworth et. al. JVSTA

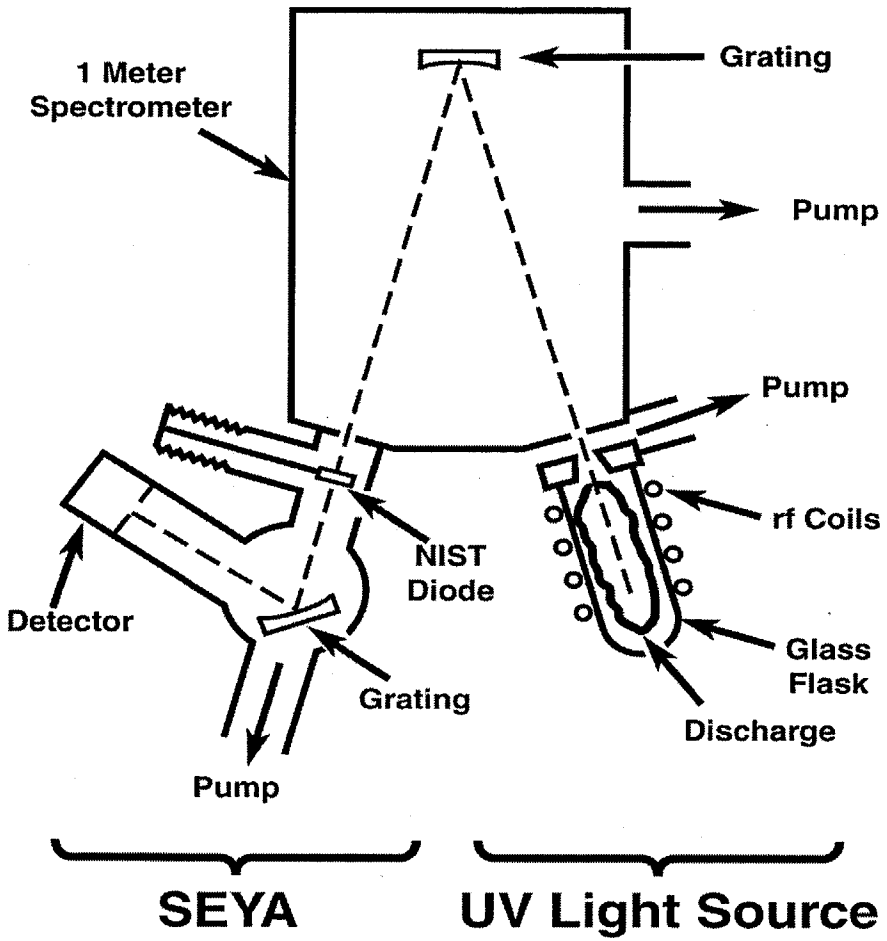

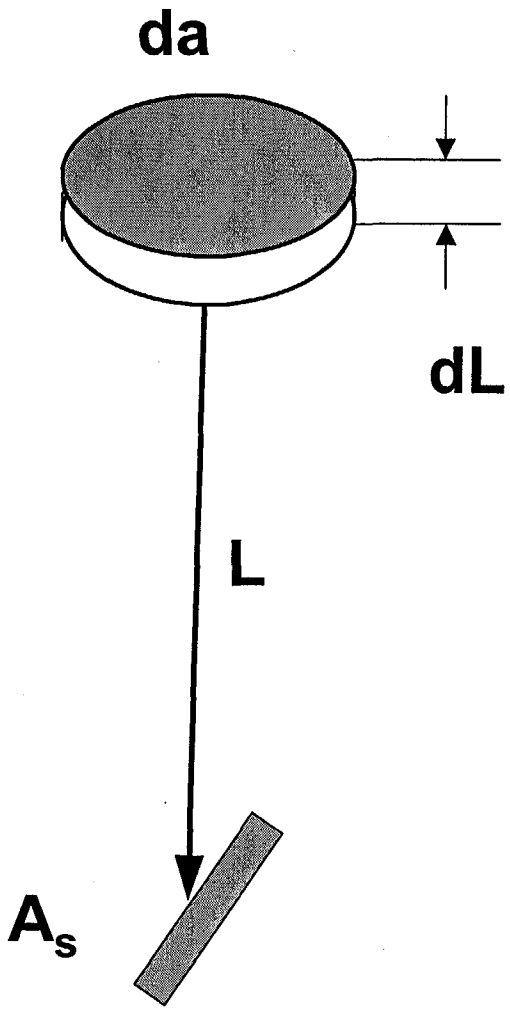

Figure 5: J. R. Woodworth et. al. JVSTA

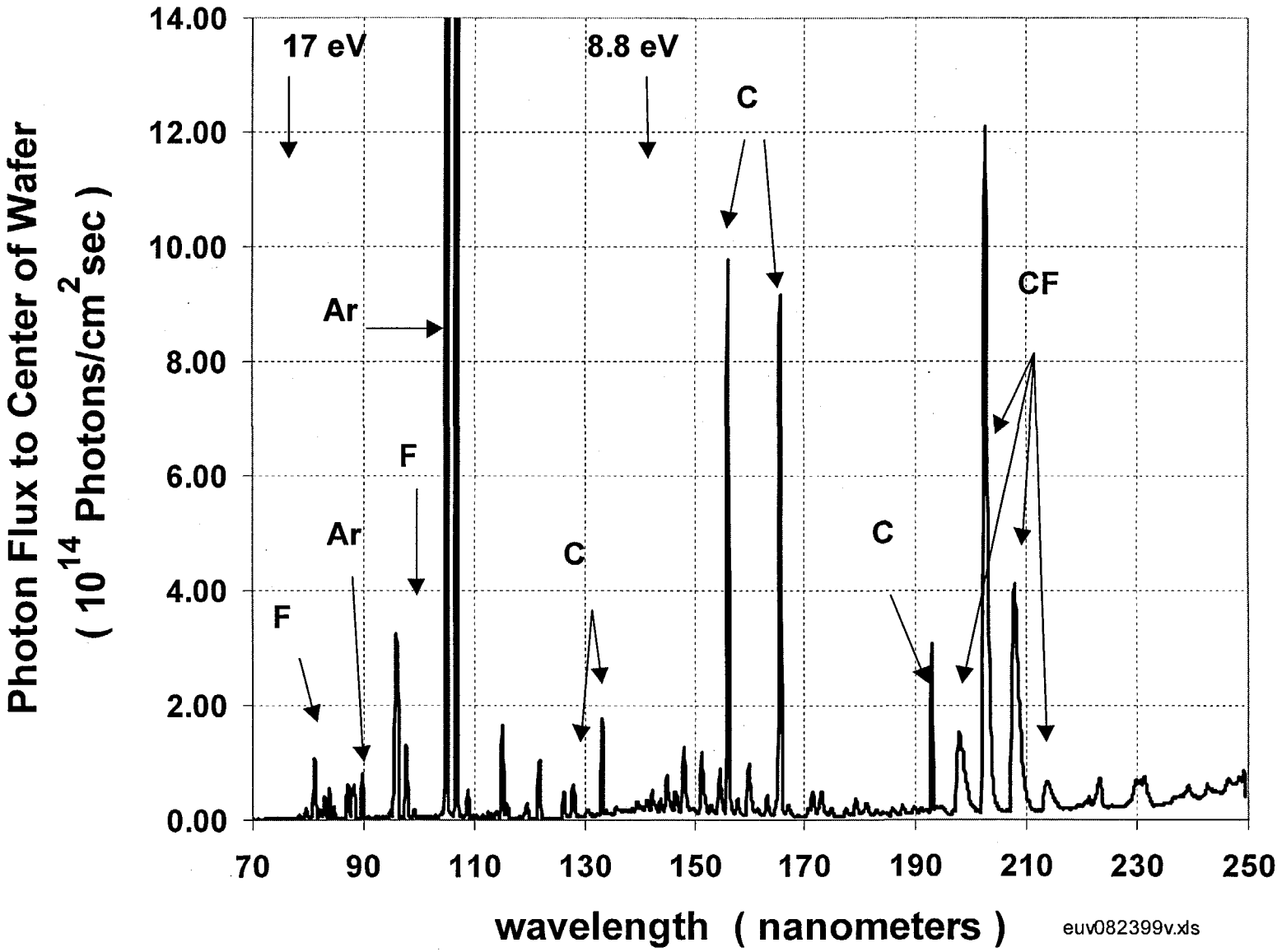

Figure 6, J. R. Woodworth et. al. JVSTA

Figure 7, J. R. Woodworth et. al. JVSTA

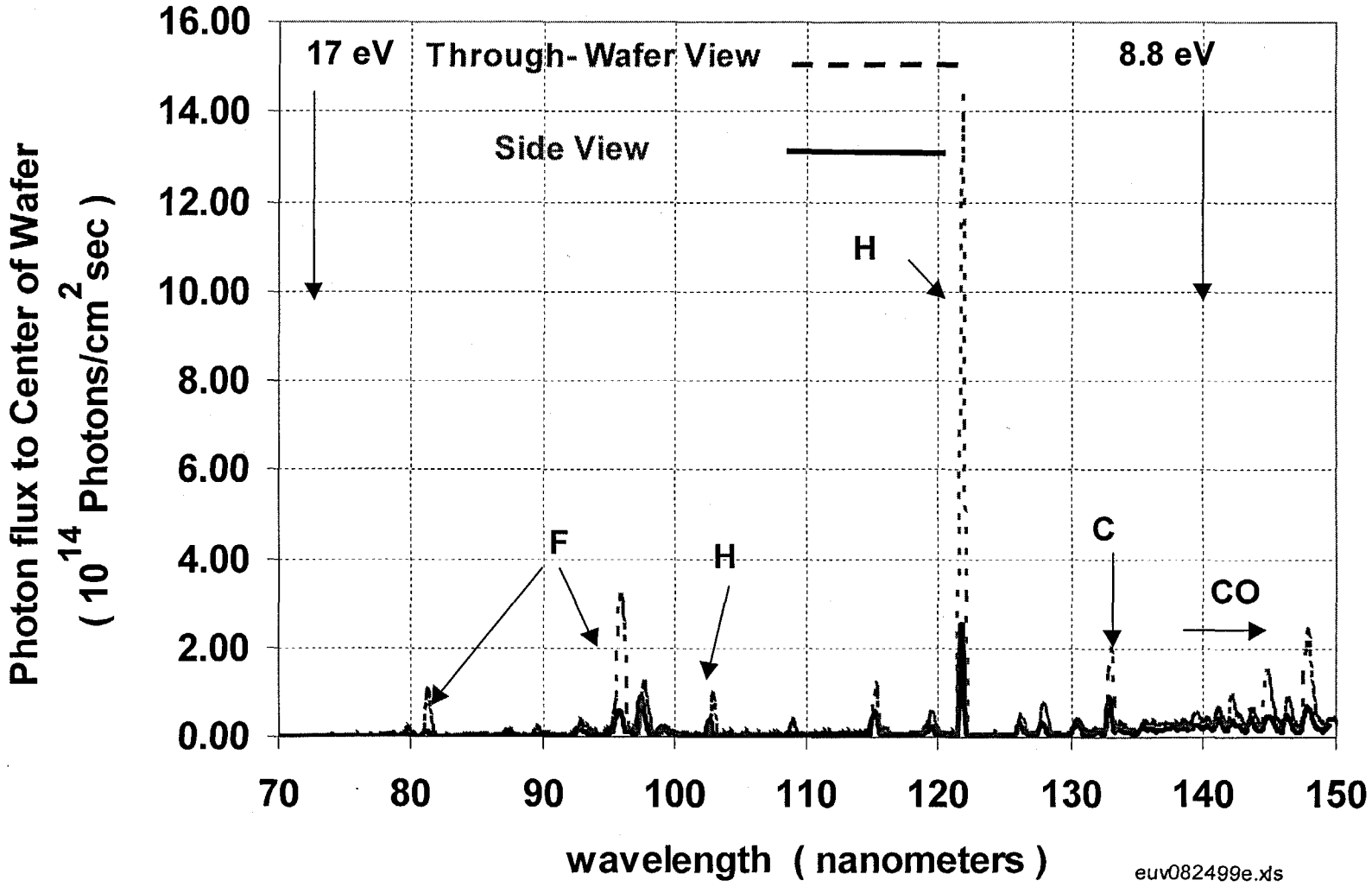

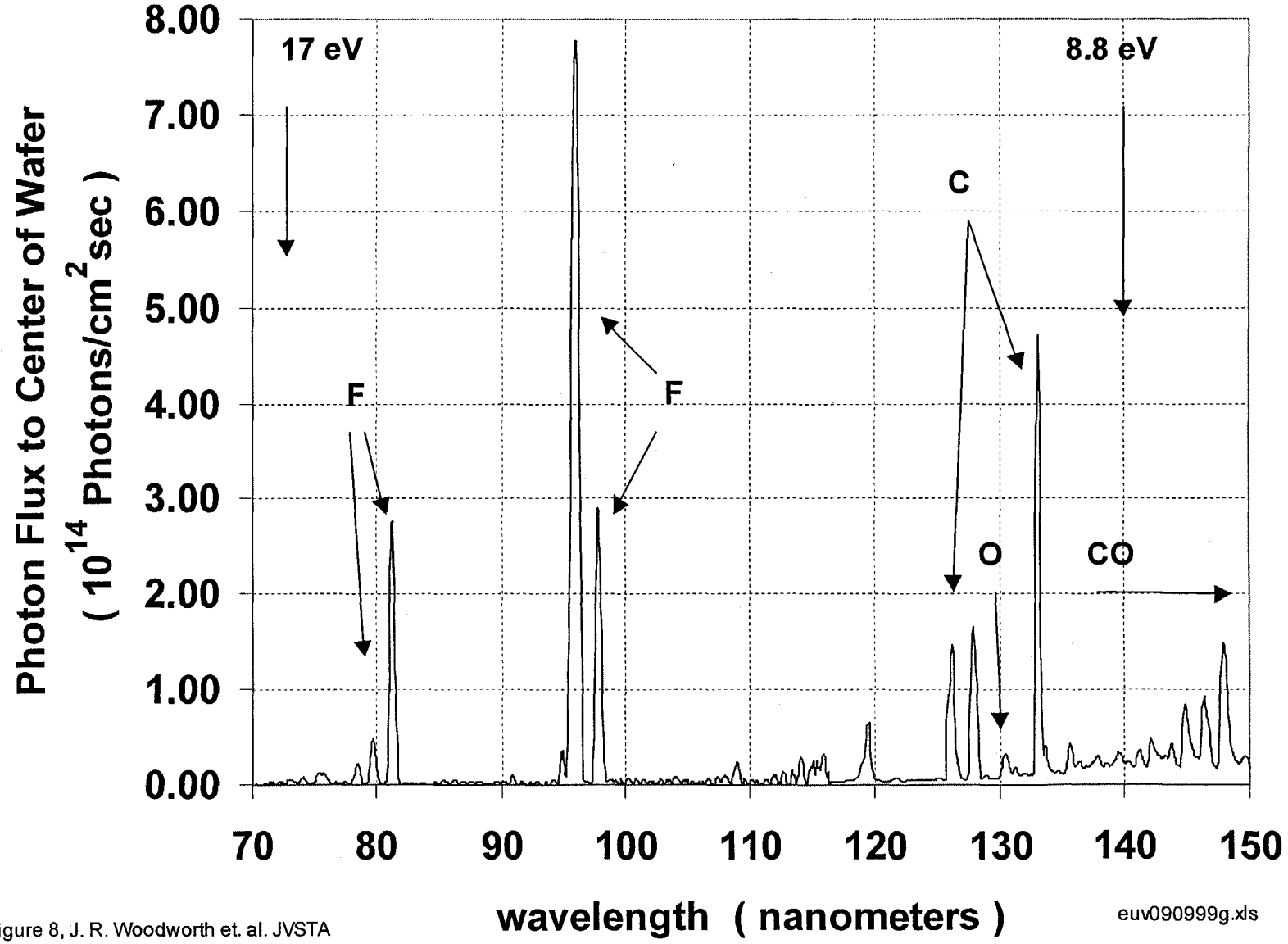

Figure 8, J. R. Woodworth et. al. JVSTA

Figure 9, J.R. Woodworth et. al, JVSTA

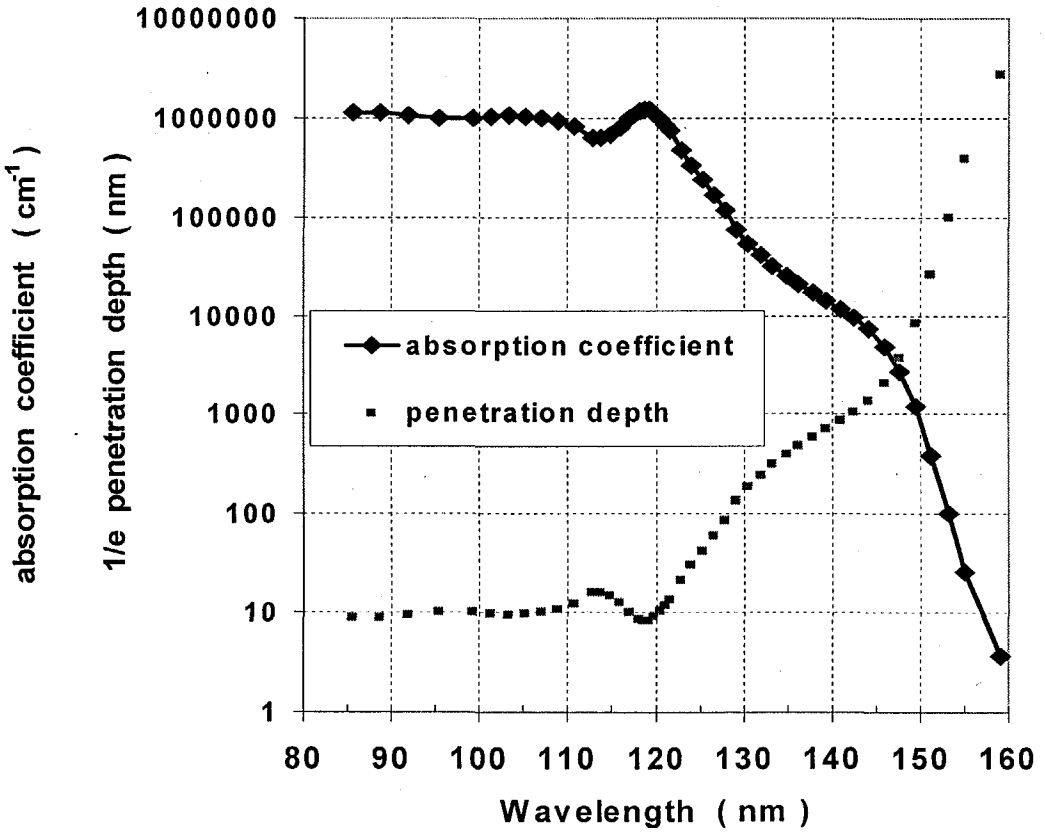

quartz absorption coeffs.xls